CrystEngComm

Controlling water structure and behavior: Design principles from metal organic nanotubular materials

Journal:	*CrystEngComm*
Manuscript ID	CE-HIG-03-2020-000331.R1
Article Type:	Highlight
Date Submitted by the Author:	17-Apr-2020
Complete List of Authors:	Applegate, Lindsey; University of Iowa, Department of Chemistry Forbes, Tori; University of Iowa, Department of Chemistry

SCHOLARONE™
Manuscripts

For submission to CrystEngComm

Controlling water structure and behavior: Design principles from metal organic nanotubular materials

Lindsey C. Applegate and Tori Z. Forbes*

Department of Chemistry, University of Iowa, Iowa City, IA 52242

* Corresponding author: tori-forbes@uiowa.edu

Abstract

Water contained within nanoporous spaces possesses different chemical and physical properties than what is observed in the bulk phase, and these differences are exploited in the natural world to impart specific functionalities to biologic and geologic systems. The goal of rational design is to take this inspiration from nature and develop an understanding of structure-function relationships to create materials with similar or improved level of control. In this highlight, we explore the similarities between water confined within synthetic metal organic nanotubular materials and natural systems. We focus first on water structure and unique hydrogen bonding nets and then move to the observed differences in water behavior between nanoconfined and bulk systems. Last, we discuss specific design principles that should be explored to control the structure and properties of water under confinement within metal organic nanotubular materials.

Introduction

The chemistry that happens within nanopores differs widely from that of bulk solutions and has importance to the function and processes that we observe within natural systems. In general, the variations that exist for nanochemistry arise from the drastic increase in the surface area to volume ratio when something is reduced to the nanoscale.[1] This change results in the surface energy becoming a larger component of the energetics, varies the electronic properties, and alters the chemical and physical properties of the material. [1-3] These surface effects can also be observed with the inverse condition, when atoms, ions, or molecules are confined to a nanoscale space, pore, or channel. Just as with nanoparticles, confinement within nanosized channels results in deviations in the chemical and physical behavior when compared to the bulk. These nanochannels exist all around us and have implication for the chemistry that controls the natural world. Nanoporous spaces are observed within protein channels, lipid bilayers, diatomaceous materials, iron oxide minerals, grain boundaries, clays, and organic rich shales and many of these regions are considered high energy environments with enhanced reactivity.[4-6]

Water is also ubiquitous in the natural world and is often observed within these nanoconfined environments, which leads to unique chemistry within these systems. As with other molecules, the confinement of water within nanoscale pores leads to deviations in the thermodynamics and physical properties compared to the bulk, including variations in the freezing point, density, surface tension, and dielectric constant.[7-10] Many of these changes are related to changes in the hydrogen bonding networks that occur between water molecules and may cause forms that are generally thermodynamically unstable in the bulk to form more readily.[7] The importance of these confinement effects within biological and geological systems are becoming an area of significant study and variations from the bulk are drastic. For example, unusual ordering of water has recently been reported under nanoconfinement, including forms that typically only exist within cold subduction zones and deep space (Ice-VII).[11-13] Unusual behavior was also noted within the beryl mineral phases with quantum tunneling observed for the hydrogen atoms on the water molecule confined within the 0.5 nm pore space.[14] Within biologic systems, the role of water to control the dynamic and functionality of biological molecules is well known.[15] Their ability to engage in supramolecular orientation of biomolecules within nanoenvironments is now moving to the forefront of efforts to develop a better understanding of biological processes.[16] A well-known example of important nanoconfinement effects is within aquaporin channels, which are transport

proteins located with the cell wall that can selectively move water between the membrane while excluding charged ions.[17] These proteins are found in all kingdoms of life and many, such as human aquaporin 1 (AQP1), utilize a passive gating mechanism that involves a confined channel and a local electrochemical potential.[18] The water moves through the channel as a single column of molecules at a surprising rate of 3 x 10^9 water molecules per second per subunit.[17]

One of the goals of crystal engineering and rational design of materials is to take inspiration from these natural systems and create novel materials where we can now control these properties for use in advanced applications and technologies. Within engineered materials, there is a wide array of materials that have been developed that have the required nanoporous spatial confinement regions. Mesoporous silica, [7, 19-22] carbon nanotubes,[23-43] zeolites, [20, 44-50] polymers,[43, 51-55] and composites[22, 52, 56-58] represent classifications of materials that have traditionally been explored for nanoconfinement effects. The typical pore size that has been targeted for investigations of nanoconfinement effects ranges from 5-20 Å, but the major focus within these studies are molecular dynamics, phase changes, gas storage, and catalytic performance.[59-64] Confinement effects associated with water have also been evaluated and confirm deviation from bulk like behavior. Diffusion of water through synthetic nanopores is also enhanced, although the exact amount has differed significantly depending on the study. Holt *et al.*[65] indicated rates in carbon nanotubes that were 560-8400 times as large as those of Hagen-Poiseuille flows, where Majumder *et al.* [38] reported rates that were 3-5 times faster than bulk. Phase behavior within synthetic nanopores have also been reported to be impacted by nanoconfinement and can lead to the formation of supercooled water and glassy transition states at lower temperature regimes (150-227 K).[55, 66, 67]

Studies on synthetic materials suggest that the surface chemistry of the internal pore wall is important and can influence the hydrogen bonding network that occurs between the confined water molecules. Hydrophobic surfaces, such as single walled carbon nanotubes, force the water molecules to engage in hydrogen bonding with neighboring water molecules to create ordered structures with an ice-like array when confined to pores that are 0.8-2 nm in diameter.[26, 27, 33-37, 39, 40, 68, 69] Theoretical studies have postulated the variety of structural arrangements for water within hydrophobic nanoconfinement may also be dependent on the overall size of the nanotube and the temperature and pressure regimes.[25, 29, 32, 66] Hydrophilic surfaces can engage with additional polar and hydrogen bonding interactions and directly impact the molecular structure associated with the

surface.[32, 70] This often leads to variations in the bond strength because a subset of water molecules are strongly bound to the interior walls, whereas less restricted water molecules are more mobile throughout the remaining channel space.[71] Mixed confinement includes both hydrophilic and hydrophobic regions, such as those observed in proteins and aquaporin channels, but there is a lack of experimental systems and systematic studies for these types of materials.

Metal-organic materials represent a newer classification of materials that can also be used to explore confinement effects and have a controllable crystal engineering aspect that can lead to a more nuanced understanding of the chemistry within confined spaces. Metal-organic materials are porous, hybrid materials where building blocks are constructed from metal centers connected by bridging organic linkers.[72] This synthesis can be conducted in a variety of ways, and tunability of the material allows for synthesis according to inclusion of the desired guest molecule and the dimensionality of the structural topology. Significant efforts initially focused on the three-dimensional metal organic frameworks with the discovery of MOF-5 by Yaghi and coworkers.[73] This area of crystal engineering quickly exploded to include tens of thousands of new compounds based upon the premise and success of rational design principles. More recently, there is a push towards low dimensional metal organic materials due to increased mass transfer within these materials that could improve catalytic and energy storage applications. Low dimensional metal organic materials include zero-, one-, and two-dimensional topologies with fixed coordinate parameters in the nanoscale.[74] Zero-dimensional structure refers to nanoclusters which can be arranged into hierarchical structures with nano- and mesoporous cavities. Increasing the dimensionality to 1-D metal organic materials leads to the formation of nanowires, rods, and ribbons, but nanoporous structures include hollow nanowires or macrocycles that are bonded through supramolecular interactions to create related nanotubular structures. These nanotubular structures can provide the appropriate diameter (0.5-2.0 nm) to explore the effects of nanoconfinement of water molecules. In addition, they provide the opportunity to rationally design surface hydrophobicity to create a range of materials with spatial variation in the polar or nonpolar functionalities that can lead to a better understanding of surface effects in water confinement and development of controllable properties.

In the current highlight, we first identify a subset of metal organic nanotubular materials that have been reported to contain unusual ordered water confined within 1-D pore spaces. Next, unusual physical and chemical behavior of the water confined within metal organic materials is

described and finally, we summarize future design principles and opportunities. This highlight builds from the review of water adsorption within metal organic frameworks by Canivet *et al.* which was focused on applications in adsorbent-based chillers and material for enhanced proton conduction. [75] In addition, we also point interested readers to a review article by Jia and Zheng that provides a comprehensive look at metal organic nanotubular materials that are known to date and the major synthetic pathways for developing these phases.[76]

Water structure within metal organic nanotubular materials

While the number of metal organic framework materials numbers in the tens of thousands, there are only 76 reported metal organic nanotubular compounds reported in the literature as of March 2020. Within this body of work, the number of times ordered water is mentioned is much higher than that of other metal organic materials, where disordered solvent molecules are usually noted and, in many cases, structurally unrefined. This may be due to the overall engineering and the application of these materials because many MOFs are designed to have large surface areas that can allow rapid diffusion and storage of gases and not confine the molecules. In this section, we will describe the metal organic nanotubular materials (broadly defined) that report ordered water molecules. We include metal organic frameworks and supramolecular structures that contain nanoscale 1-D pore spaces as metal organic nanotubular phases and provide additional insight into the behavior of nanoconfined water. Throughout this section we will explore structural topologies of these water nets and compared to those networks observed within natural systems.

One of the first nanotubular metal organic materials to report unusual water structure is that of Fei *et al*. in 2005 (Fig. 1), where they utilized a zwitterionic linker to create a coordination polymer that housed a water channel.[77] [Zn(L)BrH2O]·H_2O (L = imidazolium dicarboxylate) contains Zn^{2+} cations in a tetrahedral coordination with the linker molecule connecting the metal nodes together to form the helical nanotubular motif with a channel diameter of 0.5 nm. Within the channel, the water molecules are engaged in strong hydrogen bonding (D-H…A = 2.728-3.261 Å) to the interior wall, but weaker interactions (D-H…A = 2.955Å) amongst themselves to form a 1-D water chain. The authors noted the similarities between the water chain within this synthetic compound and that of aquaporin channels and noted that the internal diameter of the nanotubular material is same size as the narrowest region of the pore in the protein. However, aquaporins have

more extensive hydrogen bonding between the encapsulated water molecules than what is observed in the synthetic compound.

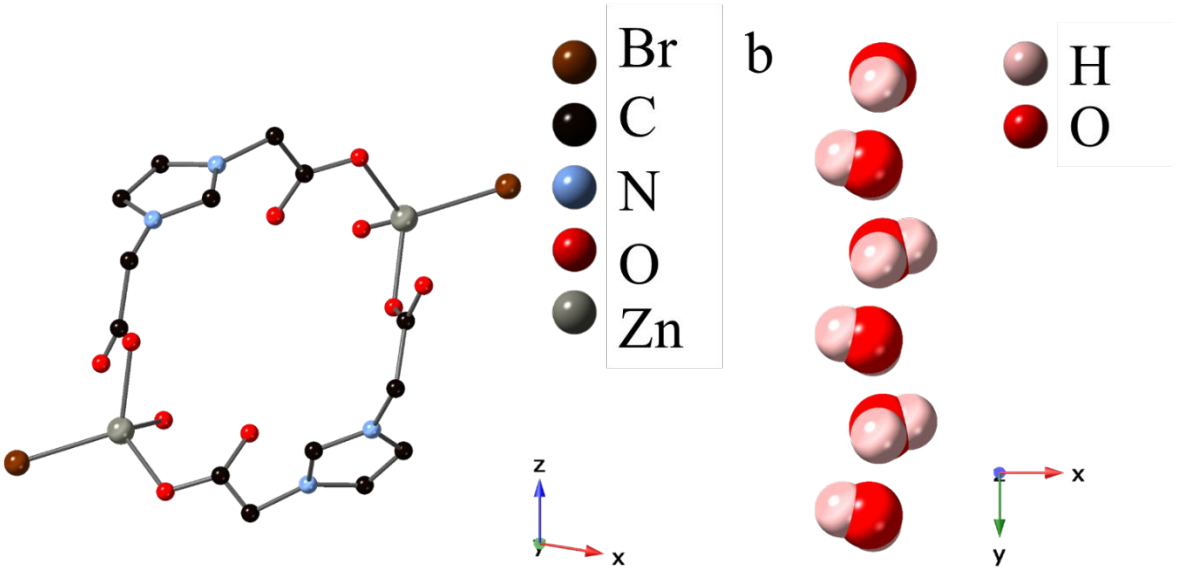

Figure 1. View of $[Zn(L)BrH_2O]\cdot H_2O$ down the channel of the nanotube (a) and the isolated water network (b).[77] The water chain extends down through the nanotubular pore and engages in hydrogen bonding with the wall of the nanotube.

Similar water wire nets were noted in the case of Huang *et al.* within $[Cd_3(phen)_3(HL)_2(H_2O)_2] \cdot 4.25\ H_2O$ (L = p-terphenyl-type 4,4′-(1,4-phenylene)bis(2,6-dimethyl-3,5-pyridinedicarboxylic acid) (Fig. 2).[78] This material is constructed from the supramolecular interaction of individual one-dimensional Cd nanotubes that have a 6^3 topological framework. There are two separate channels within this material that are 1.3 and 0.55 nm in diameter and the authors considered the interior walls to be hydrophilic. Within the smaller space, water wires are observed that contain two different helical motifs. The water molecules themselves are engaged in strong H-bonding interactions (D-H..A = 2.682 or 2.852 Å) along the length of the tubes and possess either left-handed (*meso*) or right-handed (*plus*) pseudo screw axes. Based upon the pitch parameters, the quasi-periodic structures of the water chains were designated as a "Bernal spiral". Within solid ice phase diagram, Ice-XII also contains a screw-type hydrogen-bonded arrangement that is a right-handed helix. The bulk Ice-XII structure contains additional hydrogen bonding to

create an extended lattice, although the network is typically disordered and readily converts to the stable Ice-I (I_h) form.[79]

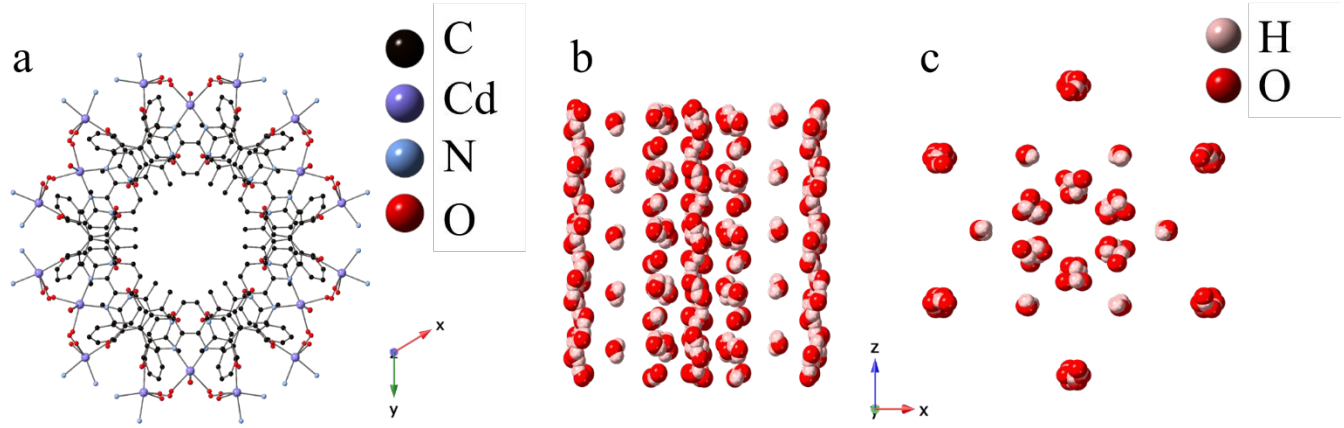

Figure 2. The 1.3 nm nanotube within $[Cd_3(phen)_3(HL)_2(H_2O)_2] \cdot 4.25\ H_2O$ (a) is arranged using supramolecular forces to form a structure consisting of two channels that encapsulate right and left-handed water chains.[78] The structure of the water molecules are seen along the *y* axis (b) and the *z* axis (c).

Within larger pore spaces, helical water wires with more pronounced curvature can be observed, as were noted in the case of Zn(*l*-LCl)(Cl)]$(H_2O)_2$, [Zn(*l*-LBr)(Br)]$(H_2O)_2$, [Zn(*d*-LCl)(Cl)]$(H_2O)_2$, and [Zn(*d*-LBr)(Br)]$(H_2O)_2$ (L = 3-methyl-2-(pyridin-4-ylmethylamino)butanoic acid] that was described by Sahoo *et al.* (Fig. 3).[80] The metal nodes and organic linkers arrange themselves into parallel 1-D helical channels (diameter of 1.2 nm) along the crystallographic *c*-axis. Within these channels, water wire nets engage with hydrogen-halogen interactions (D-H...A = 3.158 and 3.175 Å for Cl and Br, respectively) to the interior walls and spiral in a helical fashion along the length through weak hydrogen bonding interactions between the water molecules (D-H...A = 3.34 Å). The water wires mimic the chirality of the interior walls, which is based upon the exact isomer of the linker molecule.

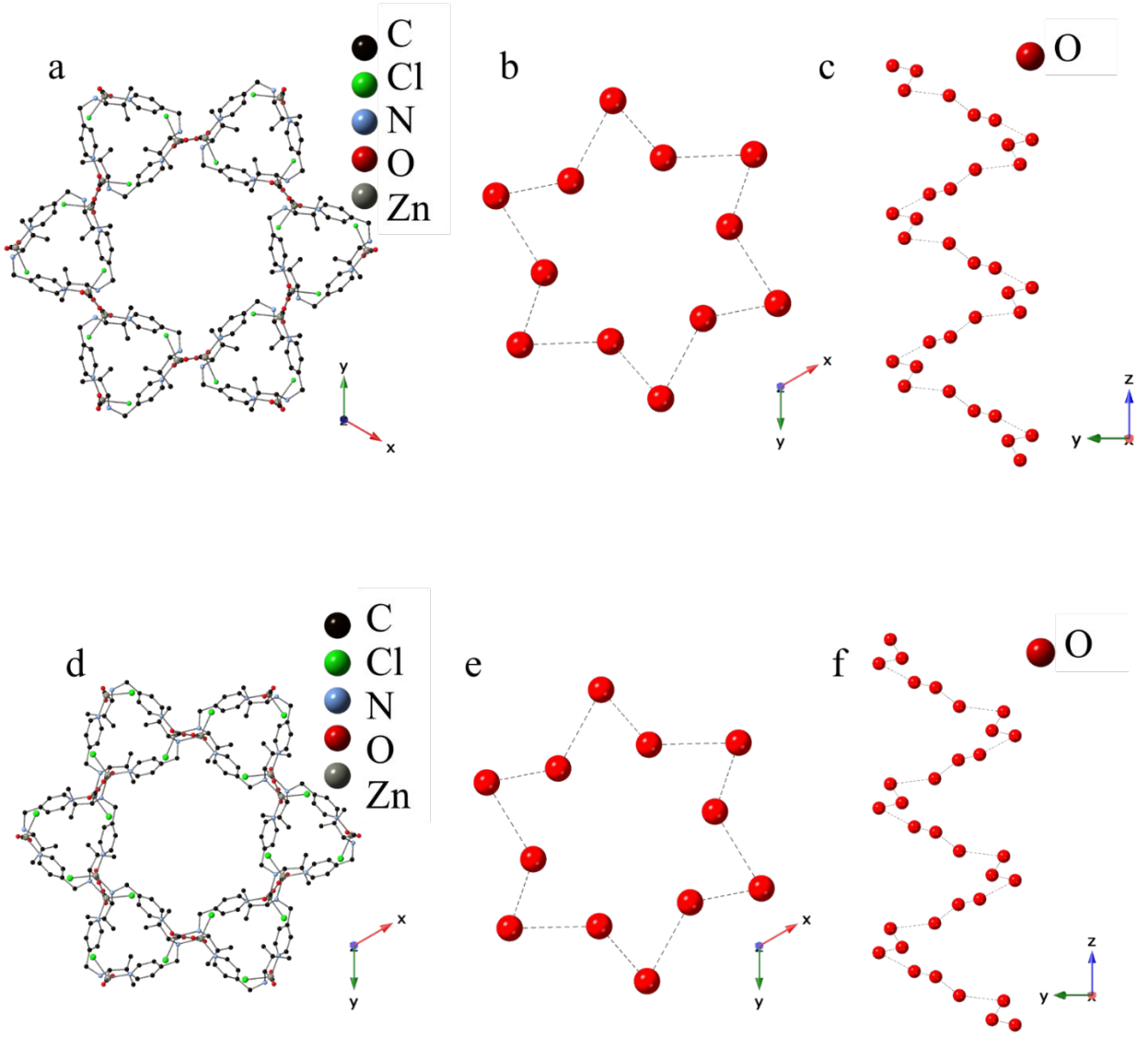

Figure 3. Zn(*l*-LCl)(Cl)]$(H_2O)_2$ (a) and Zn(*d*-LCl)(Cl)]$(H_2O)_2$ (d) and their water networks (b/c and e/f, respectively), where the helicity of the water chain is dependent on the chirality of the ligand.[80] Bromine isomers of each were also synthesized and exhibit the same water networks.

A helical water structure is observed in the case of $[(UO_2)_3(L)_2(O)_2(OH)_2](H_2O)_6$ (L = glycine), where the glycine molecule provides directed self-assembly of the confined water molecules (Fig. 4).[81] The nanotubular structure itself is composed of uranyl glycine coordination polymers that then engage in additional charge assisted hydrogen bonding interactions to form a lattice with a 1-D pore space of 1.35 nm. The water molecules engage in strong hydrogen bonding interactions among themselves (D-H...A = 2.80 and 2.97 Å) to create quasi-hexagonal arrangement

that extended in a helical fashion along the interior of the nanotube. Additional H-bonds (D-H...A = 2.65 – 2.83 Å) anchor the water helix to the interior walls. This leaves a void space within the channel of 0.8 nm, which was likely filled with solvent during the crystallization process but was rapidly removed upon isolation from the mother liquor.

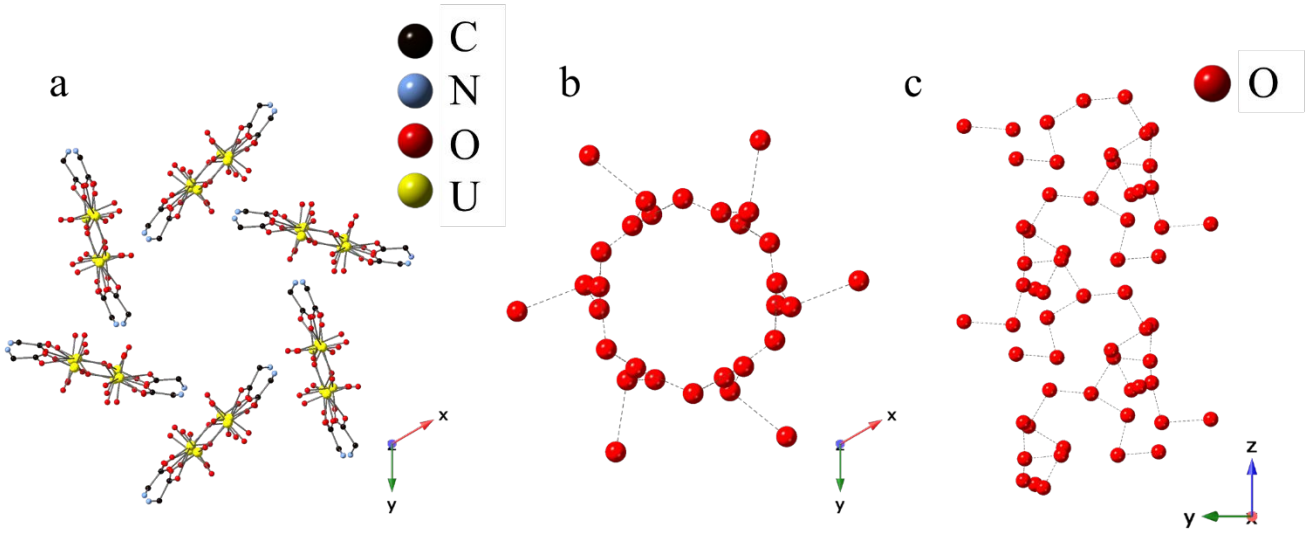

Figure 4. The $[(UO_2)_3(L)_2(O)_2(OH)_2](H_2O)_6$ compound contains a nanotubular pore (a) and the hydrogen bonding network of water molecules (b and c) is located within the 1.35 nm pore.[81]

Chen *et al.* observed a similar motif with strong interaction between the water molecules and the interior channel walls that anchored additional water molecule in the interior of the pore space (Fig. 5).[82] The compound $[La(H_2O)_4[La(L)(H_2O)]_3 \cdot 12\ H_2O]$ (L = 1,3-propanediaminetetraacetate) and its dehydration products are built upon eight membered La^{3+} rings and form 1-D channels with a 1.0 nm diameter. Within the channels, there are extended water nets that contain twelve and six member rings. The twelve membered rings are anchored to the interior wall through hydrogen bonding networks with the ligand (D-H…A = 2.629-2.677 Å). Additional H bonding interactions occur to the smaller six-member ring with D-H…A distances between neighboring water molecules of 2.818 Å. The hexagonal ring is in a chair conformation, which is similar to that observed within the Ice-I (I_h) structure.

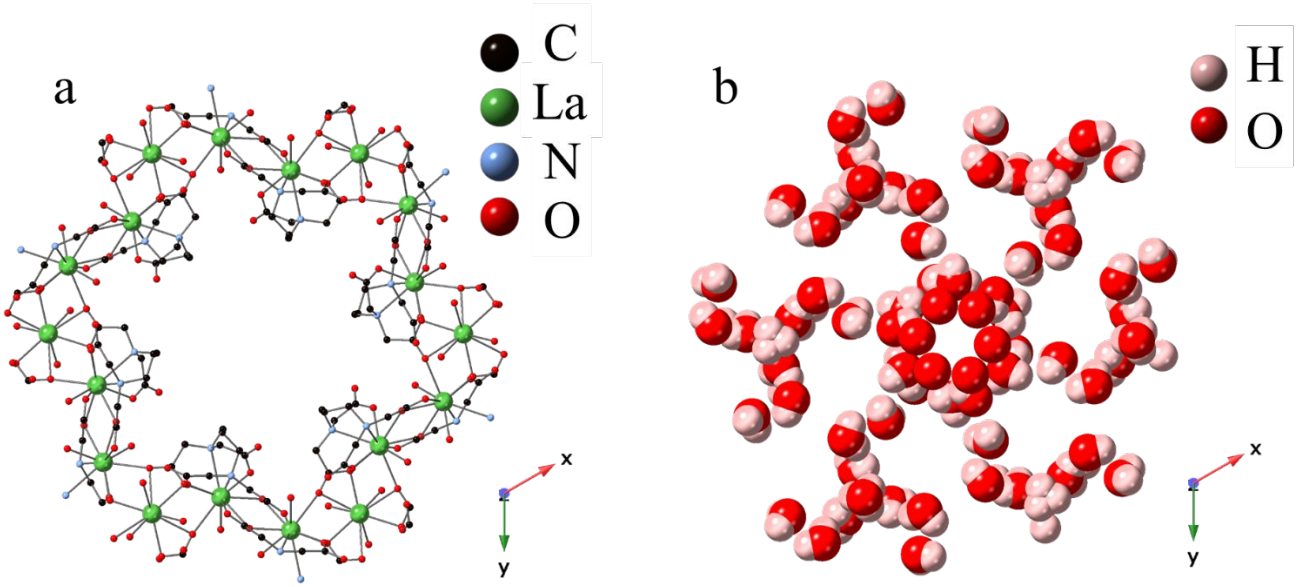

Figure 5. $La(H_2O)_4[La(L)(H_2O)]_3 \cdot 12\ H_2O$ (a) and the water network in the open channel (b) are both viewed down the z axis (direction of the pore). A hexagonal ring of water molecules is in the inner portion of the water network, while the outer portion includes water molecules bonding to the nanotubular wall via hydrogen bonding with the ligand.[82]

Other hydrogen bonded rings with varying sizes can be observed within metal organic nanotubular compounds that also rely on interactions with the interior walls as a means to anchor the water net. Dai *et al.* reported the compound $Zn(L)(bpy) \cdot 3\ H_2O$ (L = 5-amino-2,4,6-triiodoisophthalic acid) that contains 1-D square channels with dimensions of 1.11 x 0.96 nm (Fig. 6).[83] Within the channels are water molecules that are clustered into a twelve member rings. The average D-H…A distance between the water molecules is 2.761 Å and there is a separation distance of 0.95 nm between the clusters. Hydrogen bonding to the amine group of the ligand anchors the water clusters within the channel. Jin *et al.* reported the $Cd(L)2bpp_3(H_2O)]_2 \cdot 8\ H_2O$ (L = 1,3 adamantanedicarboxylic acid) compound possess 1-D channels with an internal diameter of 0.9 nm (Fig. 7).[84] Water molecules are arranged within the channels in hexagonal nets that hydrogen bond with the ligands embedded in the interior wall. D-H…A distances within the hexagons are reported as 2.996 and 2.450 Å and are again separated by a distance of 1.0 nm.

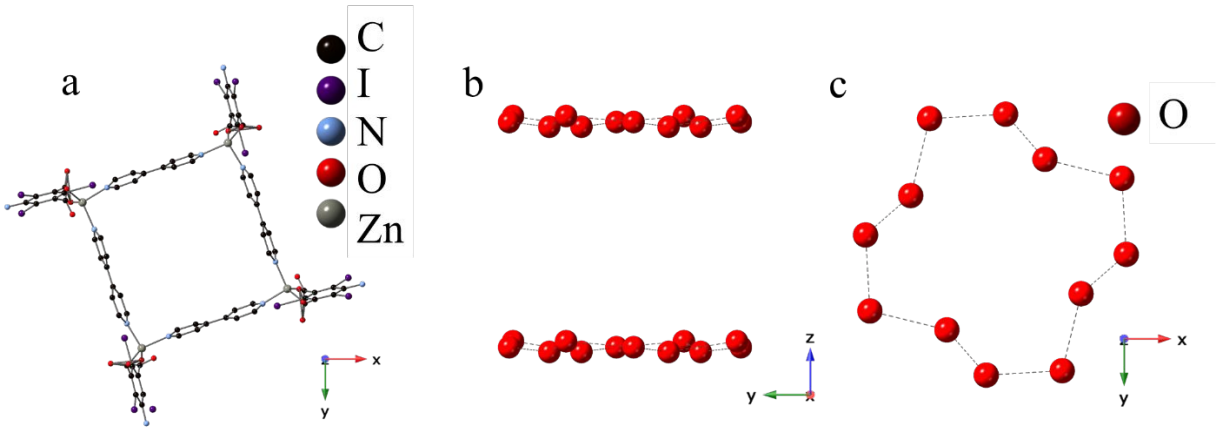

Figure 6. Zn(L)(bpy) ·3 H_2O is viewed down the *z* axis (a), which exhibits the square subunit of the nanotube. This unit is linked using the 5-amino-2,4,6-triiodoisophthalic acid ligand. The water network is shown along the x axis (b) and the *z* axis (c).[83]

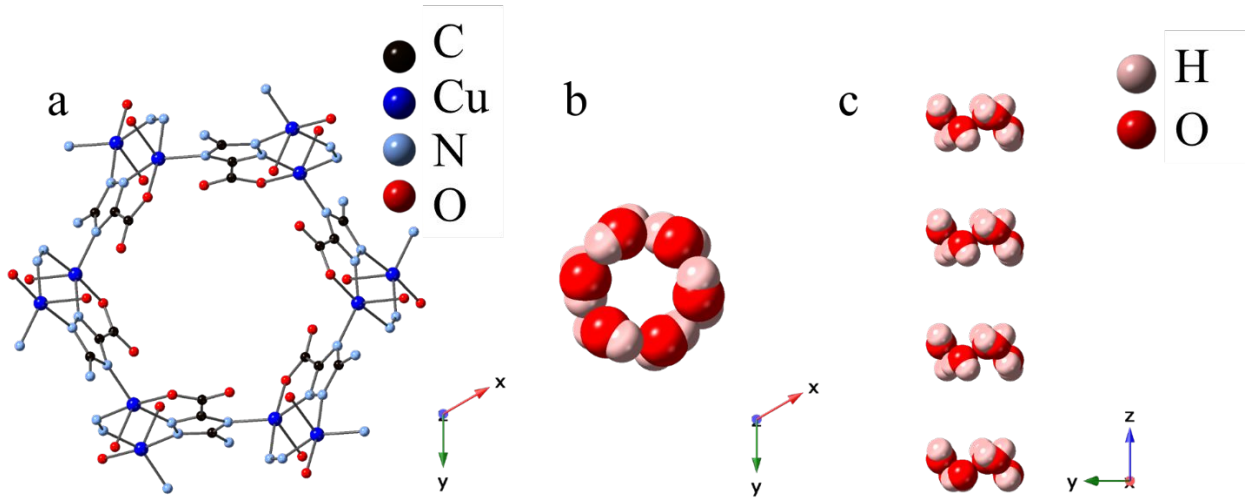

Figure 7. $Cd(L)_2bpp_3(H_2O)]_2$· 8 H_2O (a) includes hydrogen bonds between the wall and the water network (b and c). View (b) depicts the water network down the channel, while (c) is perpendicular to the 1-D pore and shows multiple layers of the hexagonal water network.[84]

Individual hydrogen bonded rings can be combined to form larger clusters that then extend along the 1-D nanochannels. For example, Cui *et al.* reported the compound $[Ru(L)_3(TMA)]$ ·DMF · 9 H_2O (L = 2,2'-biimidazole and TMA = trimesate) that has 1-D channels within internal diameters of 1.2 nm (Fig. 8).[85] A complex water network is located inside the channel that is again

stabilized by the participating in hydrogen bonding interactions with the walls of the structure (D-H…A = 2.76-2.88 Å). The authors describe the network as an aggregated $(H_2O)_{28}$ cluster in a double crown formation of cyclic water hexamers. A DMF molecule is also located within the net and engages in hydrogen bonding interactions with the confined water molecules. The average D-H…A distances between the waters in the cluster are 3.00 Å, which is longer than those of solid phases of ice.

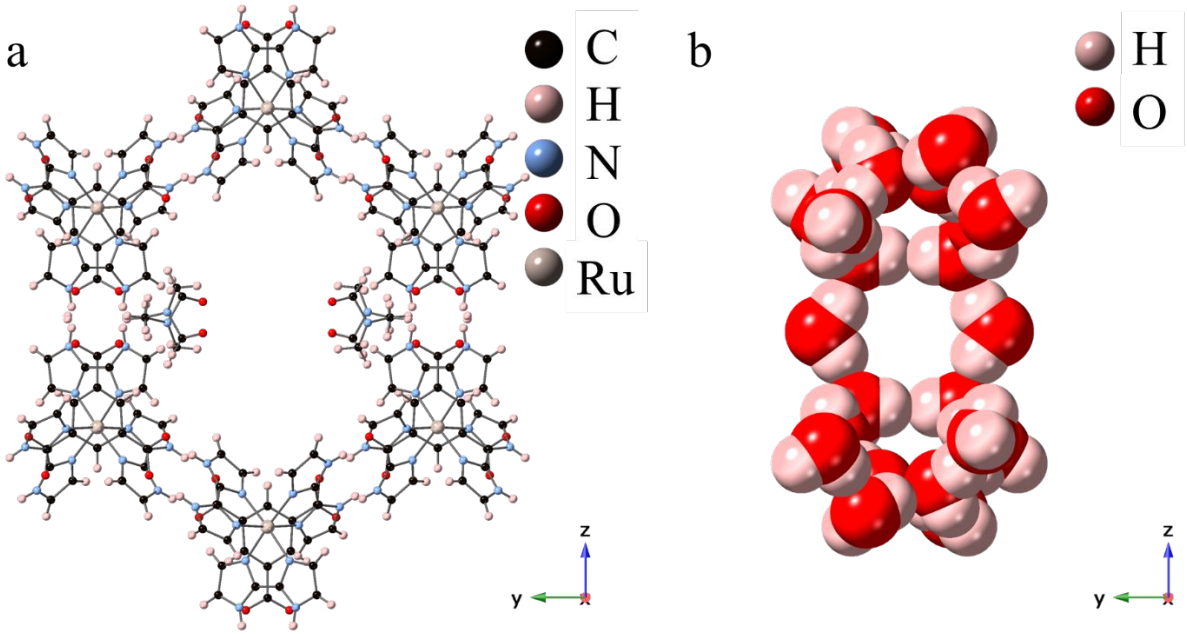

Figure 8. The 1-D channel of $[Ru(L)_3(TMA)] \cdot DMF \cdot 9\ H_2O$ (a) contains a cyclic water cluster (b). DMF molecules (not shown) are also observed within the water network and interact via hydrogen bonding with the water network.[85]

Extended structures that resemble ice-like networks have also been observed under nanoconfinement. The metal-organic nanotube $(C_4N_2H_{12})_{0.5}[(UO_2)(L)(HL)] \cdot 2\ H_2O$ (L = iminodiacetate) contains U^{6+} metal nodes and zwitterionic-like linkers (Fig. 9).[86] Structural characterization of this material revealed an ice-like array of water molecules running along the length of the 1.2 nm diameter channels (Fig. 9). There are two crystallographically distinct water molecules that are arranged in hexagonal rings with a chair confirmation with D-H…A distances between 2.79-3.10 Å. This leads to an extended Ice-I (I_h) structure that was shown to be stable after isolation from the mother liquor and at room temperature. A hydrophobic character for the

interior channel walls was postulated based upon water adsorption energies and thermal expansion parameters. The ice-like structure is also similar to those postulated to exist within single-walled carbon nanotubes and supports the idea of a hydrophobic channel that enables strong interactions to occur between the confined water molecules.

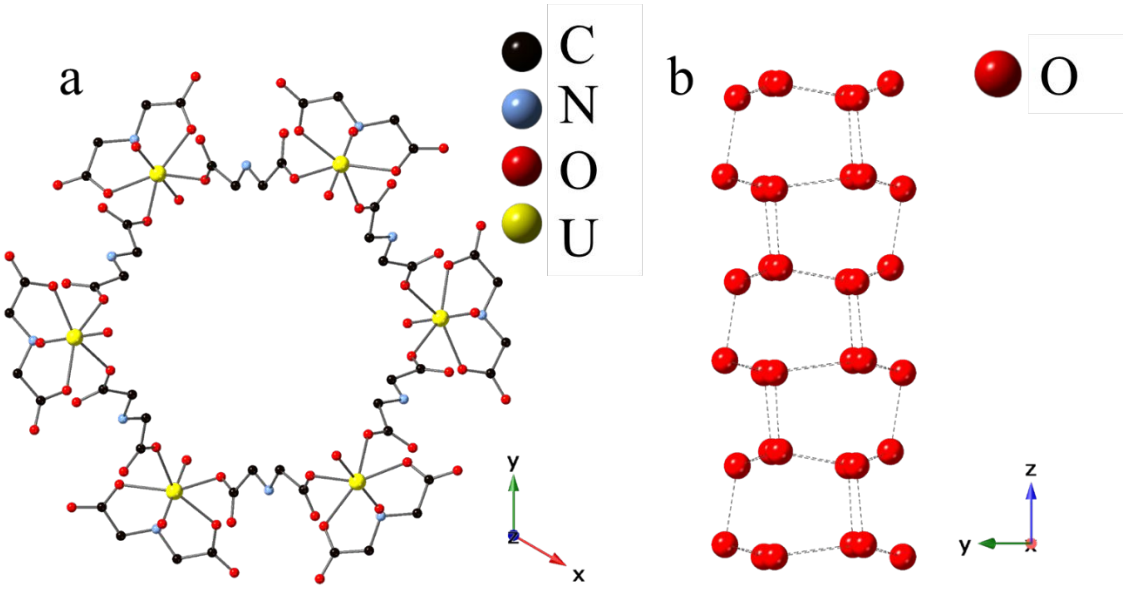

Figure 9. Macrocyclic rings form the outer walls of the $(C_4N_2H_{12})_{0.5}[(UO_2)(L)(HL)] \cdot 2\ H_2O$ nanotube structure (a), which includes piperazinium countercations between individual nanotubes (not visualized).[86] The water network (b) is an ice-like structure that sits within the channel and maintains its structure at room temperature.

Similar hydrophobic confinement was observed within $[Pt(L)(bpy)Br]_4(SO_4)_4 \cdot 32\ H_2O$ (L = 1R, 2R)-(–)-1,2-diaminocyclohexane) that was synthesized by Otake *et al* (Fig. 10).[87] The $[Pt(L)(bpy)Br]^{2+}$ units are separated by sulfate anions and the extended lattices contains two types of channels that are either hydrophobic or hydrophilic in character. Within the hydrophobic channel (Channel A) an extended network of water molecules is arranged in alternating square or octomeric nets that can be observed with D-H…A distances between 2.5-3.4 Å. The hydrophobic nature of this channel again allows for stronger interactions of the water to itself than to the interior wall (> 2.9 Å). Channel B is created between the nanotubular motifs and the sulfate anions and can be considered hydrophilic. The water within this confined space engage in strong hydrogen

bonding with the sulfate anions and two water molecules bridge the counterions to create a situation with some similarities to that of Nafion.

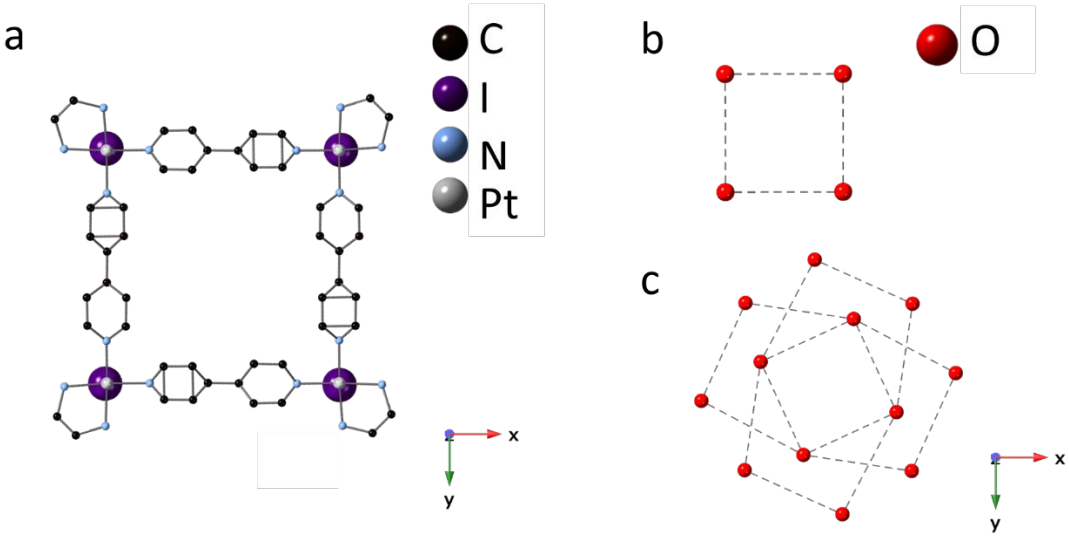

Figure 10. Isostructural representation of $[Pt(L)(bpy)Br]^{2+}$ (a) and the tetrameric (b) and hexameric (c) water networks contained within the pore. [88]

More complex water networks can be observed in the case of $\{M_2(Cu_3(L)_6)\}\cdot 8\ H_2O]$ (M = La, Nd, and Eu, L = iminodiacetate) (Fig. 11).[89] This bimetallic system contains a 1-D pore space that is 1.68 nm in diameter and contains an extended network of water molecules that the authors described as similar to a "Chinese lantern" motif. A closer look at the water net reveals that, of the twelve water molecules that make up the motif, three of them are anchored to the interior wall of the channel. Within this hydrogen bonding network, two of the water molecules interact with four others in a tetrahedral coordination and the remainder are arranged in connected five member rings. The tetrahedral coordination is observed in Ice-II (I_c) which is a meta-stable form that typically forms by condensation of water at 1 atm and -80 °C or below -38 °C in water droplets less than 6 μm.[90] The arrangement of the pentagons is similar to that observed in Ice-III where the five-membered rings are arranged as bicyclo-heptamers. This form of ice only occurs at 300 MPa and at temperatures less than -23 °C.[91]

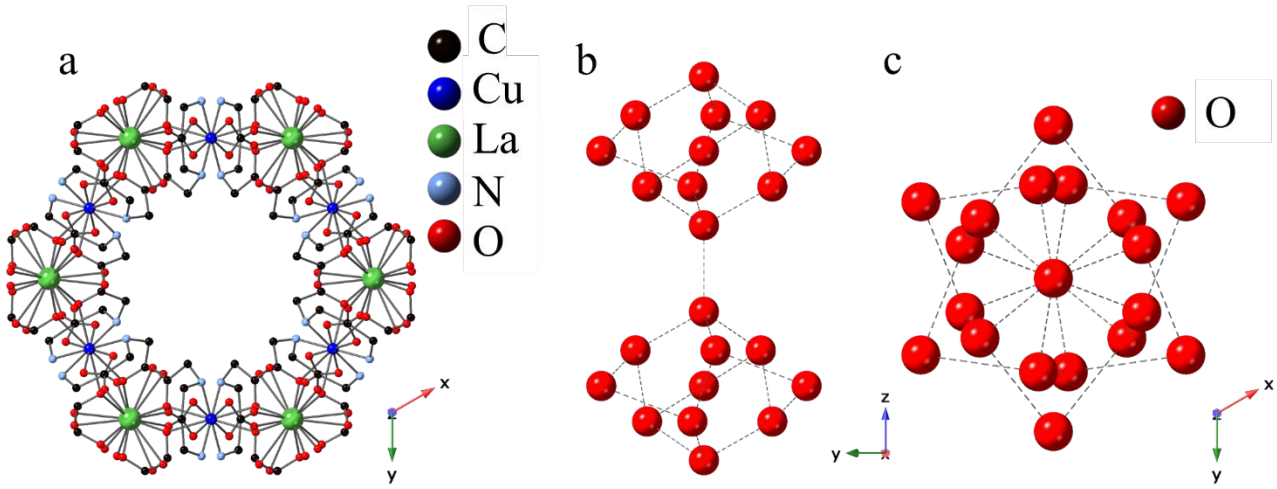

Figure 11. [{$M_2(Cu_3(L)_6)$}·8 H_2O] (M = La, Nd, and Eu, L = iminodiacetate) (a) includes a complex water network (b and c) in a "Chinese lantern" motif.[89]

Variations in physical properties of nanoconfined water molecules.

A relatively commonly investigated phenomenon associated with nanoconfinement is the resulting variations in the chemistry and behavior of water within the pores of the materials. Both computational and experimental studies have been conducted in order to probe the extent of the effects of nanoconfinement on the behavior of water when adsorbed into nanoporous cavities.[44, 92-95] In this section, we will explore the reported variation in behavior of nanoconfined water molecules within metal organic nanotubular materials. The materials and related water nets have been described in the previous section and here we will discuss details regarding changes in water adsorption and removal, diffusion, proton conductivity, and selectivity. We also describe additional studies on metal organic framework materials, zeolites, and silica-based compounds that provide additional insights into the nanotubular materials.

Thermogravimetric analysis is a technique that is widely used to evaluate or confirm the amount of material in the pore space and determine the temperature at which this solvent is released from the cavity. Removal of water from the nanotubular material typically fits within two categories depending on the interactions with the interior walls: 1) hydrophobic walls lead to lower temperature removal of water, and 2) hydrophilic walls with strong hydrogen bonding interactions to confined water molecules cause typical (100 °C) or higher temperature dehydration.

For example, complete removal of water within the more hydrophobic cavities of $(C_4N_2H_{12})_{0.5}[(UO_2)(L)(HL)]\cdot 2\ H_2O$ (L = iminodiacetate) occurs at 37 °C [86] (Fig. 12) compared to those of $[Cd_3(phen)_3(HL)_2(H_2O)_2]\cdot 4.25\ H_2O$ [96] or $Zn(L)(bpy)\cdot 3\ H_2O$ [83] where gradual removal of the strongly bound water molecules occurs over a greater range (~50-150 °C). Multilayers can also occur where outer water molecules strongly interact with interior walls and secondary interior layers engage in hydrogen bonding between neighboring water molecules. When this occurs, the thermogravimetric analysis often reveals a multi-step dehydration process. This occurs for the dehydration of $[La(H_2O)_4[La(1,3\text{-pdta})(H_2O)]_3\cdot 12\ H_2O]$ where the initial weight loss for the water within the channel occurs at 45 °C and a secondary gradual weight loss from 115-140 °C is the removal of the more strongly bound water molecules.[82]

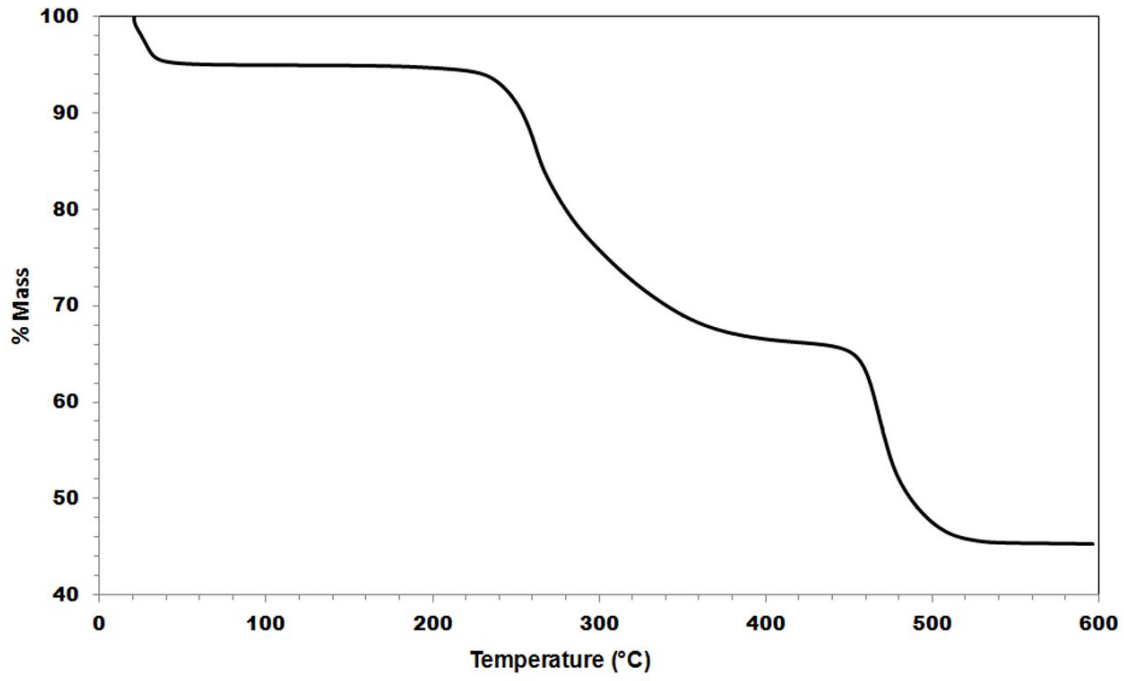

Figure 12. TGA exhibiting water removal at 37 °C from pores of $(C_4N_2H_{12})_{0.5}[(UO_2)(L)(HL)]\cdot 2\ H_2O$. The subsequent regions of weight loss are a result of degradation of the nanotubular components (iminodiacetate and piperazine). Reprinted with permission from (D. K. Unruh, K. Gojdas, A. Libo and T. Z. Forbes, *J. Am. Chem. Soc.*, 2013, **135**, 7398-7401.). Copyright (2013) American Chemical Society.[86]

The water adsorption properties for both $(C_4N_2H_{12})_{0.5}[(UO_2)(L)(HL)] \cdot 2\ H_2O$ and $[Pt(L)(bpy)Br]_4(SO_4)_4 \cdot 32\ H_2O$ [87]have been explored and demonstrate differences in the uptake behavior at different relative humidity levels. For $(C_4N_2H_{12})_{0.5}[(UO_2)(L)(HL)]\cdot 2\ H_2O$, compete hydration of the pore spaces was observed when the humidity reached 45% after 20 minutes of exposure to water vapor. A more gradual uptake of the water was observed between 0-100% relative humidity in the case of $[Pt(L)(bpy)Br]_4(SO_4)_4 \cdot 32\ H_2O$. Additional thermodynamic studies for $(C_4N_2H_{12})_{0.5}[(UO_2)(L)(HL)] \cdot 2\ H_2O$ indicated that the dehydration enthalpy was 57.8 ± 1.9 kJ/mol, which is higher than that of the vaporization enthalpy for water (44 kJ/mol) but lower than most zeolites that contain cations within the interior cages (61.3 – 84.9 kJ/mol). Based upon this information, the interaction between the confined water molecules and the interior walls of the nanotube was calculated at 7.8 ± 0.95 kJ/mol. The energy of this interaction is within the range of one weak hydrogen bonding interaction and further supports the hydrophilic nature of the interior wall for this compound.

These dehydration and water uptake results are similar to what is observed in theoretical studies on related porous materials. Gomez-Alvarez *et al*. utilized Monte Carlo simulations to explore hydrophobic zeolitic imidazolate frameworks (ZIFs), zeolite (LTA-5A), and mesoporous silica.[44] Within the LTA-5A compound, the confined water molecules interact strongly with the cations (specifically Ca^{2+}) that are also contained within the confined spaces. In the ZIF material, interactions between the interior wall and the confined water molecules were found to be most prevalent at low pressures, but after condensation is reached, the water-water interactions become more important. The mechanism of adsorption also varied based upon interactions with the interior walls of the nanochannels and water-water interactions are enhanced by the hydrophobic character of the interior walls and the formation of nanoscale cavities. This study also indicated that the thermodynamics of water adsorption was affected by the peculiarities of the pore structure, namely the ability to engage in hydrogen bonding interactions.

Serre *et al*. and Medders and Paesani further investigated behavior of nanoconfined water molecules in porous metal organic frameworks using molecular dynamic simulations (Fig. 13).[93, 97] MIL-53(Cr) was shown to engage in a breathing behavior that resulted in reversible change in the diameter of the pores with water loading. The pores narrowed with the introduction of a few water molecules, and then return to their wider state as the number of water molecules increased inside the channel. Additional investigations indicated that the specific behavior of the water

molecules with the interior walls of channel influenced this behavior. Supported by the calculated linear and non-linear infrared spectroscopy results, Medders and Paesani determined that the initial introduction of water to the channels resulted in strong interactions with the interior walls.[93] The initial loading of four water molecules per unit cell caused the confined water molecules to be "pinned" into a 1D nanowire through interaction with the bridging hydroxide groups on the interior walls. As the loading increases and the water molecules became more closely packed together, the network of water-water hydrogen bonding became stronger. This was also reflected in the calculated IR spectra because the -OH stretching bands red-shifted with increasing water content in the 1-D channels. The large channel diameters for the MIL-53(Cr) material are similar to the nanotubular metal organic material that contain multilayers of water and we predict that similar behavior and spectroscopic signals would be observed in those cases.

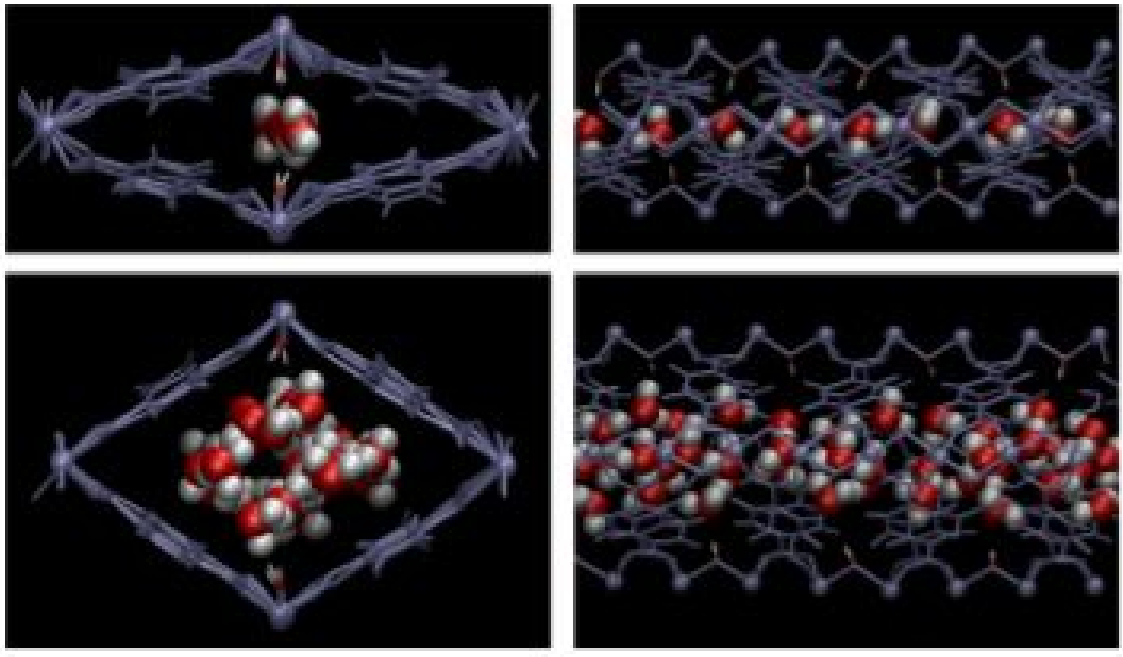

Figure 13. Computational efforts to describe water adsorption behavior was performed on a metal organic framework (MIL-53(Cr) . When a small amount of water molecules was introduced into the pore, the diameter is narrowed (top). Increasing the number of water molecules results in a wider pore diameter and causes the channel to "breathe" (bottom). Similar features may be observed within metal organic nanotubular materials. Reprinted with permission from (G. R.

Medders and F. Paesani, *J. Phys. Chem. Lett.*, 2014, **5**, 2897-2902.). Copyright (2014) American Chemical Society.[93]

The importance of the interactions between water molecules and the functional groups on the interior wall of the channel is also noted in the diffusion rates of the water within these confined spaces. Jayasinghe *et al.* provided experimental values for the diffusion of water within the 1-D nanochannels of $(C_4N_2H_{12})_{0.5}[(UO_2)(L)(HL)]\cdot 2\ H_2O$ and reported diffusion coefficient of 1.2 x 10^{-12} cm^2/sec.[98] This is much slower than what is observed for single walled carbon nanotubes (10^{-5} to 10^{-6} cm^2/s) and is actually closer to the value for low density amorphous ice ($1x10^{-11}$ (170K to $2x10^{-14}$ (60K) cm^2/s). Aquaporin channel diffusion has also been determined at $3.6x10^{-6}$ cm^2/s.[99] Placing this nanotubular material in context with other types of channels also provides experimental evidence that the chemistry of the interior walls is important in controlling the movement of the nanoconfined water molecules. As stated earlier, interior channel walls of $(C_4N_2H_{12})_{0.5}[(UO_2)(L)(HL)]\cdot 2\ H_2O$ can be considered hydrophobic based upon the interaction energies. However, this is also supported by the crystal structure determination because the interior walls are lined with hydrophobic $-CH_3$ groups and the uranyl oxo (which has been shown to be a poor Lewis base and hydrogen bond acceptor). This structure is unique in that there are also double-protonated amine groups pointing towards the exterior of the channel. This leads to no hydrogen bonding interactions with the confined water molecules, but does provide electrostatic interactions that could stabilize the water rings located within the channel. These electrostatic interactions may decrease the water diffusivity within the confined space to that of a more ice-like behavior. This is different that the purely hydrophobic channels in single-walled carbon nanotubes, that exhibit enhanced movement throughout material.[98]

The movement of water is also important for proton conductivity within 1-D nanochannels and enhanced proton conductivity has been noted in a couple of instances. Within $[Pt(L)(bpy)Br]_4(SO_4)_4 \bullet 32\ H_2O$, proton conductivity measurements of 1.7 x 10^{-2} S cm^{-1} were reported by Otake *et al*.[87] Proton diffusivity was anisotropic and was reported as 2.9 x 10^{-11} to 1.7 x 10^{-12} m^2/sec through the nanochannels. Conductivity value became larger with increasing relative humidity, which is indicative of the important role of the confined water molecules for the observed conductivity values. The authors also suggested that the mechanism for transport was not mobile hydronium ions, but shuttling between water molecules located within the channel.

Sahoo *et al.* also explored proton connectivity within Zn(*l*-LCl)(Cl)]$(H_2O)_2$, [Zn(*l*-LBr)(Br)]$(H_2O)_2$, [Zn(*d*-LCl)(Cl)]$(H_2O)_2$, and [Zn(*d*-LBr)(Br)]$(H_2O)_2$ and observed differences based upon subtle variations in the material. Higher proton conductivity of 4.45 x 10^{-5} and 4.42 x 10^{-5} S cm^{-1} was noted for Zn(*l*-LCl)(Cl)]$(H_2O)_2$ and [Zn(*d*-LCl)(Cl)]$(H_2O)_2$, whereas zero conductivity was measured for the Br^- based materials. The authors suggested that electronegativity difference between Cl^- and Br^- may explain the variations because stronger O-H…Cl-M interactions results in increasing acidity of the water proton.

Selectivity was also another important parameter that was explored with 1-D nanotubular materials. Chen *et al.* evaluated the ability of $[La(H_2O)_4[La(L)(H_2O)]_3 \cdot 12\ H_2O]$ to selectively remove water molecules from an ionic solution as a means to use this material for desalination applications.[82] In this case, they saw a linear increase in the total dissolved solids (as a proxy for salinity) upon sequential addition of the solid to a solution containing sodium chloride. Solvent selectivity was also observed in the case of $(C_4N_2H_{12})_{0.5}[(UO_2)(L)(HL)]\cdot 2\ H_2O$. Jayasinghe *et al.* performed batch solution and vapor experiments on this material using common solvents, such as acetone, methanol, ethanol, THF, DMSO, and DMF, and uptake was evaluated using thermogravimetric analyzer equipped with an evolved gas analyzer.[86, 100] No evidence of solvent uptake was observed under these conditions. The importance of interior functional groups embedded within the pore wall was also observed in other systems, such as purely organic nanotubular materials. Huang *et al.* synthesized endo-functionalized nanotubes with mixed hydrophilic (quaternary amines) and hydrophobic (naphthalene groups) regions that were further evaluated for selectivity.[78] Surprisingly, this material preferred hydrophilic molecules over hydrophobic molecules of similar shape and related MD simulations demonstrated that it was the specifics of the hydrogen bonding capabilities and hydrophobic nature of the different region of the cavity that led to this specificity.[101]

Evaluating design principles that control water structure and properties.

As we seek to predict and control water structure and mobility through metal organic nanotubular materials, we can first turn to nature for our initial understanding. As discussed in the introduction, aquaporin channels display remarkable selectivity to water molecules and fast transport. If we take a look at the structural features of one common type (AQP1), we notice an

hour-glass shape with the narrowest point comparable to the van der Waals diameter of water (2.8 Å).[102] Water molecules move through the hydrophobic channel in a single column and engage in hydrogen bonding interactions to form a single water wire. At the constriction point, a highly positive arginine residue (Arg-195) repels solvated cations and hydronium molecules.[103] Arg-195 is preserved in all aquaporins, but the position of the histidine residue (His-180) can vary and further restricts the pore diameter with an additional partial positive charge at neutral pH.[17] Two additional asparagine residues are typically located in the narrowest part of the channel and also contribute to the electrochemical gating because it forces water reorientation that restricts the ability of hydronium to pass through the opening.[102, 104] All of these features combine in a sophisticated way to create a highly selective system with excellent water transport properties, but it is really the atomistic design principles that lead to the desired effect.

From the structural exploration of metal organic nanotubular materials, we can also conclude that subtle differences in channel diameter do provide controls on water structure and properties. Smaller pores (~0.5 nm), such as those observed in aquaporin channels, $[Zn(C_7N_2O_4H_7)BrH_2O]\cdot H_2O$, and $[Cd_3(phen)_3(HL)_2(H_2O)_2] \cdot 4.25\ H_2O$, form water wires whereas larger channels (0.8-2 nm) create larger water networks. The diameter of the channels does make a difference in water properties, as Otake *et al*. noted that the fast proton conductivity exhibited within $[Pt(L)(bpy)Br]_4(SO_4)_4 \bullet 32\ H_2O$ is not observed within the related compound Pt(L)(CN) that has smaller channel diameters that are below the nanoconfinement regime (0.2 nm).[105]

As with aquaporin channels and in other synthetic systems, we also note that the surface chemistry of the interior metal organic nanotubular walls is particularly important in controlling water structure, mobility, and selectivity within metal organic nanotubular materials. Variations in the nature and strength of bonding within polar (hydrophilic) or non-polar (hydrophobic) regions of the cavity can lead to very different behavior depending on the exact interactions with the nanoconfined water molecules. Much of the unique chemistry associated water itself is related to the ability and strength of the molecule to engage in hydrogen bonding, but under confinement there is an interplay between the energy minimization of the hydrogen bonding network and interactions with the pore surface.[31] This is observed in multiple studies where strong hydrogen bonding interactions lead to ordering of the water molecules within the material, but slow transport within the pore space. Within hydrophobic spaces, the water mobility increases and the more "ice-like" structures can be formed because the interaction between water molecules is favored over

interactions with the non-polar surface groups. Mixtures of the hydrophobic and hydrophilic groups within these materials leads to the type of selectivity that is observed within aquaporin channels.[17] Water selectivity is observed in the $(C_4N_2H_{12})_{0.5}[(UO_2)(L)(HL)]\cdot 2\ H_2O$ compound and although the mechanism has not be definitely determined, it is likely due to the interplay of hydrophilic and hydrophobic groups that controls the extended hydrogen bonding network and selectivity.[86] Therefore, design principles should consider specific placement of these groups in the design of specific properties (e.g. fast vs. slow water diffusion).

We also note that in many of these compounds, the hydrophilic regions contain either carboxylate or amine groups. These are also functional groups that are observed within amino acids and engage in strong hydrogen bonding interactions. In addition, many of these hydrophilic regions have electrostatic interactions as well because the amine group is protonated and provides some level of zwitterionic-like character to the molecules. Placement of the hydrophilic groups also is an important consideration, with stabilization occurring with strongly bound water groups on the interior walls. However, it is also important to note that weaker electrostatics can also occur when the zwitterionic ligand is located on the exterior of the channel that can still result in stabilization of the confined water groups.

One other important feature that must also be considered within synthetic crystalline material is the influence of the bulk surface. Currently there are no studies that systematically investigate the importance of crystal surfaces for 1-D nanotubular materials, but Velasco *et al*.[92] provides some important initial evidence within the zeolitic imidazolium framework material, ZIF-8, to support this idea. In this study, polyaminobecylamine (PABA) was added to the hydrophobic ZIF-8 surface to introduce an element of hydrophilicity to the surface and allow for the diffusion of ionic species through the framework. NMR experiments were used to evaluate pore characteristics and diffusion coefficients, as well as the molecular density of the adsorbate. The metal organic framework, Al-MIL-96, was used as a comparison to look at the hydrophobic character of both ZIF-8 and ZIF-coated with PABA, as MIL-96 has hydrophilic pores. This allows for water to exist in two environments – both in intra- and intermolecular space. The ZIF material has $-CH_3$ moieties in the pore windows, making it hydrophobic, but as PABA is introduced, the hydrophilic nature increases. This allows for diffusion of water into the pores, and exchangeable adsorption on the surface with the PABA polymer. An increase in PABA results in an increase in

diffusion coefficient, indicating a profound effect from the surface chemistry of the crystalline material.

Additional studies are necessary to fully explore the nature of nanoconfinement within metal organic nantobular materials and to systematically evaluate structure-function relationships within these series of compounds. As mentioned earlier, the targeted design of metal organic nanotubular material is challenging but offers substantial ways to control the channel diameter and the hydrophobicity of the resulting material. Based upon our understanding of aquaporin channels, an atomistic level of control in placement of hydrophobic/hydrophillic moieties and/or charged functional groups is crucial to creating water structure and mobility. These materials offer the possibility of creating new water purification and storage materials that could provide lower cost desalination, novel energy exchange technology, and universal contaminant removal processes. In addition, exploring the chemical and physical processing occurring under nanoconfinement within these synthetic materials allows us to continue to explore these unique spaces within our natural world.

Acknowledgements

We acknowledge support from the NSF Division of Materials Research CAREER award (DMR1252831).

References

1. Y. W. Guozhong Cao, *Nanostructures and Nanomaterials*, 2011.
2. G. A. Ozin, *Adv. Mater.*, 1992, **4**, 612-649.
3. A. Malouche, G. Blanita, D. Lupu, J. Bourgon, J. Nelayah and C. Zlotea, *J. Mater. Chem. A*, 2017, **5**, 23043-23052.
4. C. Cao and Y.-T. Long, *Acc. Chem. Res.*, 2018, **51**, 331-341.
5. Y. Wang, C. Bryan, H. Xu and H. Gao, *Geology*, 2003, **31**, 387-390.
6. N. Peng, S. He, Q. Hu, B. Zhang, X. He, G. Zhai, C. He and R. Yang, *Mar. Pet. Geol.*, 2019, **103**, 456-472.
7. A. W. Knight, N. G. Kalugin, E. Coker and A. G. Ilgen, *Sci. Rep.*, 2019, **9**, 8246.
8. S. Senapati and A. Chandra, *J. Phys. Chem. B* 2001, **105**, 5106-5109.
9. T. Takei, K. Mukasa, M. Kofuji, M. Fuji, T. Watanabe, M. Chikazawa and T. Kanazawa, *Colloid Polym. Sci.*, 2000, **278**, 475-480.
10. H. K. Christenson, *J. Phys.: Condens. Matter*, 2001, **13**, R95-R133.
11. D. Shin, J. Hwang and W. Jhe, *Nat. Commun.*, 2019, **10**, 286.
12. C. R. Bina and A. Navrotsky, *Nature*, 2000, **408**, 844-847.
13. L. Zeng and D. Sasselov, *Astrophys. J*, 2014, **784**, 96.

14. A. I. Kolesnikov, G. F. Reiter, N. Choudhury, T. R. Prisk, E. Mamontov, A. Podlesnyak, G. Ehlers, A. G. Seel, D. J. Wesolowski and L. M. Anovitz, *Phys. Rev. Lett.*, 2016, **116**, 167802.
15. R. Cooke and and I. D. Kuntz, *Annu. Rev. Biophys. Bioeng.,* 1974, **3**, 95-126.
16. L. M. Alarcón, J. A. Rodríguez Fris, M. A. Morini, M. B. Sierra, S. A. Accordino, J. M. Montes de Oca, V. I. Pedroni and G. A. Appignanesi, in *Membrane Hydration: The Role of Water in the Structure and Function of Biological Membranes*, ed. E. A. Disalvo, Springer International Publishing, Cham, 2015, DOI: 10.1007/978-3-319-19060-0_7, pp. 161-187.
17. D. Kozono, M. Yasui, L. S. King and P. Agre, *J. Clin. Invest.*, 2002, **109**, 1395-1399.
18. E. Tajkhorshid, P. Nollert, M. O. Jensen, L. J. W. Miercke, apos, J. Connell, R. M. Stroud and K. Schulten, *Science*, 2002, **296**, 525+.
19. M. Baum, F. Rieutord, F. Juranyi, C. Rey and D. Rébiscoul, *Langmuir*, 2019, **35**, 10780.
20. B. Coasne and D. Farrusseng, *Microporous Mesoporous Mater.*, 2019, **288**, 109561.
21. R. Kumarasinghe, T. Ito and D. Higgins, *Anal. Chem.*, 2020, **92**, 1416.
22. R.-A. Mitran, C. Matei, D. Berger, L. Băjenaru and M. G. Moisescu, *Eur. J. Pharm. Biopharm.*, 2018, **127**, 318-325.
23. H. Ye, H. Zhang, Y. Zheng and Z. Zhang, *Microfluid. Nanofluid.*, 2011, **10**, 1359-1364.
24. T. Crouzier, A. Nimmagadda, M. U. Nollert and P. S. McFetridge, *Langmuir*, 2008, **24**, 13173.
25. A. K. Giri, F. Teixeira and M. N. D. S. Cordeiro, *J. Mol. Liq.*, 2018, **268**, 625-636.
26. K.-i. Hanami, T. Umesaki, K. Matsuda, Y. Miyata, H. Kataura, Y. Okabe and Y. Maniwa, *J. Phys. Soc. Jpn.*, 2010, **79**, 023601.
27. J. K. Holt, H. G. Park, Y. Wang, M. Stadermann, A. B. Artyukhin, C. P. Grigoropoulos, A. Noy and O. Bakajin, *Science (New York, N.Y.)*, 2006, **312**, 1034.
28. C. Hu and S. Hu, *Langmuir*, 2008, **24**, 8890-8897.
29. S. Chakraborty, H. Kumar, C. Dasgupta and P. K. Maiti, *Acc. Chem. Res.*, 2017, **50**, 2139-2146.
30. N. Karousis, N. Tagmatarchis and D. Tasis, *Chem. Rev.*, 2010, **110**, 5366-5397.
31. M. H. Köhler, J. R. Bordin, C. F. de Matos and M. C. Barbosa, *Chem. Eng. Sci.*, 2019, **203**, 54-67.
32. M. H. Köhler, J. R. Bordin, L. B. da Silva and M. C. Barbosa, *Physica A*, 2018, **490**, 331-337.
33. H. Kyakuno, K. Matsuda, Y. Nakai, R. Ichimura, T. Saito, Y. Miyata, K. Hata and Y. Maniwa, *Sci. Rep.*, 2017, **7**, 14834.
34. H. Kyakuno, M. Fukasawa, R. Ichimura, K. Matsuda, Y. Nakai, Y. Miyata, T. Saito and Y. Maniwa, *J. Chem. Phys.* 2016, **145**, 064514.
35. H. Kyakuno, K. Matsuda, H. Yahiro, T. Fukuoka, Y. Miyata, K. Yanagi, Y. Maniwa, H. Kataura, T. Saito, M. Yumura and S. Iijima, *H. Phys. Soc. Jpn.*, 2010, **79**, 083802.
36. H. Kyakuno, K. Matsuda, H. Yahiro, Y. Inami, T. Fukuoka, Y. Miyata, K. Yanagi, Y. Maniwa, H. Kataura, T. Saito, M. Yumura and S. Iijima, *J. Chem. Phys.,* 2011, **134**, 244501.
37. H. Kyakuno, H. Ogura, K. Matsuda and Y. Maniwa, *J. Phys. Chem. C*, 2018, **122**, 18493-18500.
38. M. Majumder, N. Chopra, R. Andrews and B. J. Hinds, *Nature*, 2005, **438**, 44-44.
39. Y. Maniwa, H. Kataura, M. Abe, S. Suzuki, Y. Achiba, H. Kira and K. Matsuda, *J. Phys. Soc. Jpn.*, 2002, **71**, 2863-2866.
40. Y. Maniwa, K. Matsuda, H. Kyakuno, S. Ogasawara, T. Hibi, H. Kadowaki, S. Suzuki, Y. Achiba and H. Kataura, *Nat. Mater.*, 2007, **6**, 135-141.
41. A. Zaragoza, M. A. Gonzalez, L. Joly, I. López-Montero, M. A. Canales, A. L. Benavides and C. Valeriani, *Phys. Chem. Chem. Phys.*, 2019, **21**, 13653-13667.
42. W. J. Fan and R. Q. Zhang, *J. Cluster Sci.*, 2015, **26**, 361-373.
43. K. Kaneko, T. Itoh and T. Fujimori, *Chem. Lett.*, 2012, **41**, 466-475.
44. P. Gómez-Álvarez and S. Calero, *CrystEngComm*, 2015, **17**, 412-421.
45. S. D. Chemerisov and A. D. Trifunac, *Chem. Phys. Lett.*, 2001, **347**, 65-72.
46. T. Humplik, R. Raj, S. C. Maroo, T. Laoui and E. N. Wang, *Langmuir*, 2014, **30**, 6446-6453.
47. J. Y. Kim, H. Oh and H. R. Moon, *Adv. Mater.*, 2019, **31**, 1805293.

48. P. Maheshwari, D. Dutta, S. K. Sharma, K. Sudarshan, P. K. Pujari, M. Majumder, B. Pahari, B. Bandyopadhyay, K. Ghoshray and A. Ghoshray, *J. Phys. Chem. C*, 2010, **114**, 4966-4972.
49. N. W. Ockwig, R. T. Cygan, L. J. Criscenti and T. M. Nenoff, *Phys. Chem. Chem. Phys.*, 2008, **10**, 800-807.
50. N. W. Ockwig, R. T. Cygan, M. A. Hartl, L. L. Daemen and T. M. Nenoff, *J. Phys. Chem. C*, 2008, **112**, 13629-13634.
51. K. Chrissopoulou and S. H. Anastasiadis, *Soft Matter*, 2015, **11**, 3746-3766.
52. T. Giesa and M. J. Buehler, in *Annu. Rev. Biophys.,* 2013, **42**, 651-673.
53. D. Guo, F. Zeng and B. Dkhil, *J. Nanosci. Nanotechnol.*, 2014, **14**, 2086-2100.
54. J. K. Sun, M. Antonietti and J. Y. Yuan, *Chem. Soc. Rev.*, 2016, **45**, 6627-6656.
55. E. G. Strekalova, M. G. Mazza, H. E. Stanley and G. Franzese, *J. Phys.: Condens. Matter*, 2012, **24**, 064111.
56. Z. Gao, N. Giovambattista and O. Sahin, *Sci. Rep.*, 2018, **8**, 6228.
57. X. Zhu and D. Shchukin, *Adv. Eng. Mater.,* 2018, **20**, 1800618.
58. C. Zhan, C. Lian, Y. Zhang, M. W. Thompson, Y. Xie, J. Z. Wu, P. R. C. Kent, P. T. Cummings, D. E. Jiang and D. J. Wesolowski, *Adv. Sci.*, 2017, **4**, 1700059.
59. C.-W. Chang, Z.-J. Gong, N.-C. Huang, C.-Y. Wang and W.-Y. Yu, *Catal. Today*, 2019.
60. T. Chen, P. Huo, J.-L. Hou, J. Xu, Q.-Y. Zhu and J. Dai, *Inorg. Chem.*, 2016, **55**, 12758-12765.
61. P. E. de Jongh, M. Allendorf, J. J. Vajo and C. Zlotea, *MRS Bull.*, 2013, **38**, 488-494.
62. V. Stavila, R. K. Bhakta, T. M. Alam, E. H. Majzoub and M. D. Allendorf, *ACS Nano*, 2012, **6**, 9807-9817.
63. A. Ahsan, S. F. Mousavi, T. Nijs, S. Nowakowska, O. Popova, A. Wäckerlin, J. Björk, L. H. Gade and T. A. Jung, *Small*, 2019, **15**, 1803169.
64. R. Boulé, C. Roiland, T. Bataille, L. Le Pollés, N. Audebrand and A. Ghoufi, *J. Phys. Chem. Lett.*, 2019, **10**, 1698-1708.
65. J. K. Holt, H. G. Park, Y. Wang, M. Stadermann, A. B. Artyukhin, C. P. Grigoropoulos, A. Noy and O. Bakajin, *Science*, 2006, **312**, 1034.
66. L. B. Krott, J. R. Bordin and M. C. Barbosa, *J. Phys. Chem. B*, 2015, **119**, 291-300.
67. L. Salvati Manni, S. Assenza, M. Duss, J. J. Vallooran, F. Juranyi, S. Jurt, O. Zerbe, E. M. Landau and R. Mezzenga, *Nat. Nanotechnol.*, 2019, **14**, 609-615.
68. S. Vaitheeswaran, H. Yin, J. Rasaiah and G. Hummer, *Proc. Natl. Acad. Sci. U. S. A.*, 2004, **101**, 17002-17005.
69. Y. Maniwa, H. Kataura, M. Abe, A. Udaka, S. Suzuki, Y. Achiba, H. Kira, K. Matsuda, H. Kadowaki and Y. Okabe, *Chem. Phys. Lett.*, 2005, **401**, 534-538.
70. X. Yu, H. Dong, L. Wang and Y. Li, *RSC Adv.*, 2016, **6**, 80431-80437.
71. M. I. Velasco, M. B. Franzoni, E. A. Franceschini, E. Gonzalez Solveyra, D. Scherlis, R. H. Acosta and G. J. A. A. Soler-Illia, *J. Phys. Chem. C*, 2017, **121**, 7533-7541.
72. H. Furukawa, K. E. Cordova, M. O'Keeffe and O. M. Yaghi, *Science*, 2013, **341**, 1230444.
73. H. Li, M. Eddaoudi, M. O'Keeffe and O. M. Yaghi, *Nature*, 1999, **402**, 276-279.
74. Y. C. Tan and H. C. Zeng, *ChemCatChem* 2019, **11**, 3138-3165.
75. J. Canivet, A. Fateeva, Y. Guo, B. Coasne and D. Farrusseng, *Chem. Soc. Rev.*, 2014, **43**, 5594-5617.
76. J.-G. Jia and L.-M. Zheng, *Coord. Chem. Rev.*, 2020, **403**, 213083.
77. Z. Fei, D. Zhao, T. J. Geldbach, R. Scopelliti, P. J. Dyson, S. Antonijevic and G. Bodenhausen, *Angew. Chem., Int. Ed. Engl.*, 2005, **44**, 5720-5725.
78. G.-B. Huang, S.-H. Wang, H. Ke, L.-P. Yang and W. Jiang, *J. Am. Chem. Soc.*, 2016, **138**, 14550-14553.
79. M. O'Keeffe, *Nature*, 1998, **392**, 879-879.
80. S. C. Sahoo, T. Kundu and R. Banerjee, *J. Am. Chem. Soc.*, 2011, **133**, 17950-17958.
81. J. de Groot, K. Gojdas, D. K. Unruh and T. Z. Forbes, *Cryst. Growth Des.*, 2014, **14**, 1357-1365.

82. M.-L. Chen, Y.-C. Guo, F. Yang, J.-X. Liang, Z.-X. Cao and Z.-H. Zhou, *Dalton Trans.*, 2014, **43**, 6026-6031.
83. F. Dai, H. He and D. Sun, *J. Am. Chem. Soc.*, 2008, **130**, 14064-14065.
84. J.-C. Jin, Y.-Y. Wang, P. Liu, R.-T. Liu, C. Ren and Q.-Z. Shi, *Cryst. Growth Des.*, 2010, **10**, 2029-2032.
85. Y. Cui, M.-L. Cao, L.-F. Yang, Y.-L. Niu and B.-H. Ye, *CrystEngComm*, 2008, **10**, 1288-1290.
86. D. K. Unruh, K. Gojdas, A. Libo and T. Z. Forbes, *J. Am. Chem. Soc.*, 2013, **135**, 7398-7401.
87. K.-i. Otake, K. Otsubo, T. Komatsu, S. Dekura, J. M. Taylor, R. Ikeda, K. Sugimoto, A. Fujiwara, C.-P. Chou, A. W. Sakti, Y. Nishimura, H. Nakai and H. Kitagawa, *Nat. Commun.*, 2020, **11**, 843.
88. K. Otsubo, Y. Wakabayashi, J. Ohara, S. Yamamoto, H. Matsuzaki, H. Okamoto, K. Nitta, T. Uruga and H. Kitagawa, *Nat. Mater.*, 2011, **10**, 291-295.
89. R. Ping, L.-S. Long, B.-W. Mao, Y. Yuan, R.-B. Huang and L.-S. Zheng, *Angew. Chem., Int. Ed. Engl.*, 2003, **42**, 532-535.
90. B. J. Murray and A. K. Bertram, *Phys. Chem. Chem. Phys.*, 2006, **8**, 186-192.
91. J. D. Londono, W. F. Kuhs and J. L. Finney, *J. Chem. Phys.*, 1993, **98**, 4878-4888.
92. M. I. Velasco, R. H. Acosta, W. A. Marmisollé, O. Azzaroni and M. Rafti, *J. Phys. Chem. C*, 2019, **123**, 21076-21082.
93. G. R. Medders and F. Paesani, *J. Phys. Chem. Lett.*, 2014, **5**, 2897-2902.
94. R. Renou, A. Szymczyk, G. Maurin, P. Malfreyt and A. Ghoufi, *J. Chem. Phys.* 2015, **142**, 184706.
95. A. B. Kanj, R. Verma, M. Liu, J. Helfferich, W. Wenzel and L. Heinke, *Nano Lett.*, 2019, **19**, 2114-2120.
96. K.-L. Huang, X. Liu, X. Chen and D.-Q. Wang, *Cryst. Growth Des.*, 2009, **9**, 1646-1650.
97. C. Serre, F. Millange, C. Thouvenot, M. Noguès, G. Marsolier, D. Louër and G. Férey, *J. Am. Chem. Soc.*, 2002, **124**, 13519-13526.
98. A. S. Jayasinghe, M. K. Payne, D. K. Unruh, A. Johns, J. Leddy and T. Z. Forbes, *J. Mater. Chem. A*, 2018, **6**, 1531-1539.
99. I. F. Ionenko, A. V. Anisimov and N. R. Dautova, *Biol. Plant.*, 2010, **54**, 488-494.
100. A. S. Jayasinghe, D. K. Unruh, A. Kral, A. Libo and T. Z. Forbes, *Cryst. Growth Des.*, 2015, **15**, 4062-4070.
101. T. Lohmiller, V. Krewald, A. Sedoud, A. W. Rutherford, F. Neese, W. Lubitz, D. A. Pantazis and N. Cox, *J. Am. Chem. Soc.*, 2017, **139**, 14412-14424.
102. K. Murata, K. Mitsuoka, T. Hirai, T. Walz, P. Agre, J. B. Heymann, A. Engel and Y. Fujiyoshi, *Nature*, 2000, **407**, 599-605.
103. B. L. de Groot and H. Grubmüller, *Science*, 2001, **294**, 2353.
104. E. Tajkhorshid, P. Nollert, M. Ø. Jensen, L. J. W. Miercke, J. Connell, R. M. Stroud and K. Schulten, *Science*, 2002, **296**, 525.
105. K.-i. Otake, K. Otsubo, K. Sugimoto, A. Fujiwara and H. Kitagawa, *Nature*, 2016, **55**, 6448-6451.

TOC Figure:

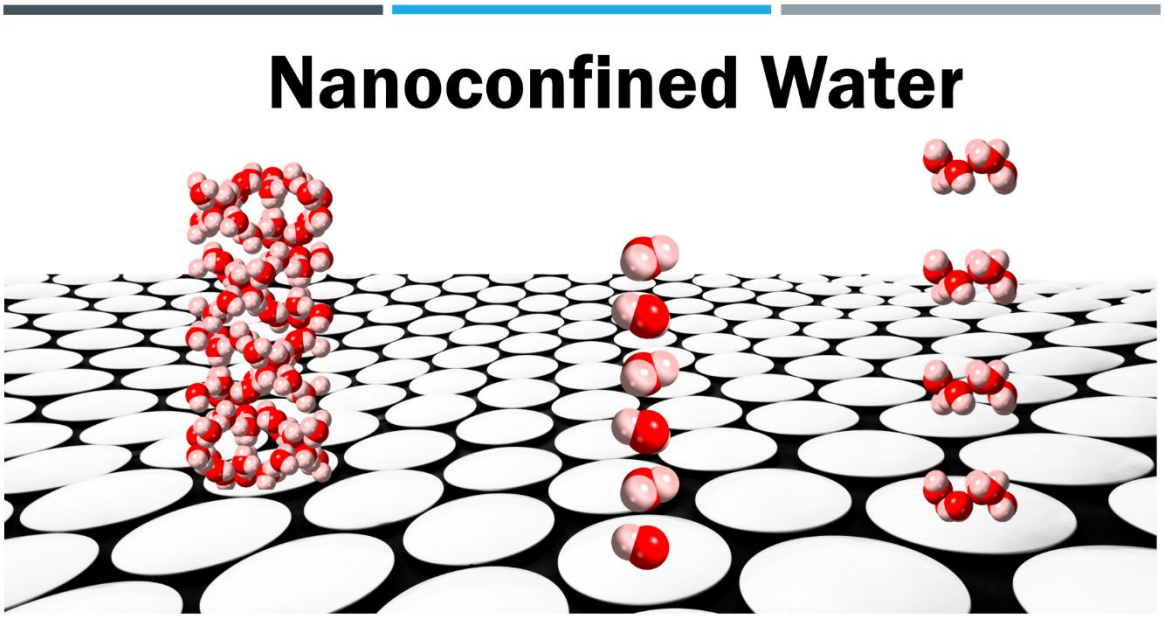

Water exhibits unique and unexpected behavioral and structural changes when confined to the nanoscale, notably within the pores of metal-organic nanotubes.